Supplementary Information (SI) for New Journal of Chemistry.
This journal is © The Royal Society of Chemistry and the Centre National de la Recherche Scientifique 2026

Supporting Information

Self-Standing Macroporous 3D Scaffold from Silk Sericin: Fabrication, Characterization, and In Vitro Bio-evaluation

Keya Mondal,[a] Sonia Agrawal,[a] Anuya Nisal,[b] Basudeb Mondal,[a] Prakash Biswas,[c] and Sayam Sen Gupta [a]*

[a] Department of Chemical Sciences, Indian Institute of Science Education and Research Kolkata, Mohanpur, 741246, India
[b] Serigen Mediproducts Pvt. Ltd., Pune, Maharashtra 411009
[c] Department of Biological Sciences, Indian Institute of Science Education and Research Kolkata, Mohanpur, 741246, India

*Email: sayam.sengupta@iiserkol.ac.in

Abbreviations

ECM	Extracellular matrix
BDE	1,4-butanediol diglycidyl ether
NaOH	Sodium hydroxide
SE1	Sericin scaffold prepared using 0.2 mM BDE
SE2	Sericin scaffold prepared using 0.36 mM BDE
SE3	Sericin scaffold prepared using 0.54 mM BDE
HFF	Human foreskin fibroblasts
FBS	Fetal bovine serum
DMEM	Dulbecco's modified eagle medium
PBS	Phosphate-buffered saline
Vm	Vancomycin
TNBS	2,4,6-trinitrobenzenesulfonic acid
MIC	Minimum inhibitory concentration
NMR	Nuclear magnetic resonance spectroscopy
FESEM	Field emission scanning electron microscope
ATR-FTIR	Attenuated total reflection mode-Fourier transform infrared spectroscopy
TGA	Thermogravimetric analysis
UV-vis	Ultraviolet-visible spectroscopy
kPa	Kilopascal
min	Minute
U mL^{-1}	Unit/mL

Materials and Methods

1,4-Butanediol diglycidyl ether, 7-hydroxycoumarin, vancomycin, and protease XIV were obtained from Sigma-Aldrich. All other chemicals used were obtained from Merck. Cocoons from *Bombyx. mori* silkworms were obtained from the Central Sericultural Research and Training Institute. HFF fibroblast cells were purchased from the National Centre for Cell Science (NCCS). The (3-(4,5-dimethylthiazol-2-yl)-2,5-diphenyltetrazolium bromide (MTT) reagent was procured from TCI. DAPI and Alexa-488 dyes were purchased from Invitrogen (Thermo Fisher Scientific). Distilled deionized water (DI, resistivity 18.2 MΩ·cm) from the Millipore Milli-Q unit was used in this study.

Instrumentation

The ^{1}H NMR spectra of extracted sericin were recorded on a Bruker Spectrometer (400 MHz) in solvent suppress mode, and signals referring to deuterated solvents (D_2O) were reported. The surface morphology of these scaffolds was analysed using a field emission scanning electron microscope (FESEM) (JEOL, JSM-5800). ImageJ software was used to determine the pore sizes (averaged from 25 random pores) within the porous scaffold. The total number of three scaffolds per group was examined. Fourier transform infrared (FTIR) analysis of these scaffolds was performed with a PerkinElmer FT-IR Spectrum GX instrument in attenuated total reflection (ATR) mode. Each spectrum was acquired by accumulation of 32 scans with a resolution of 4 cm^{-1}. IR spectra covering the amide I region (1595−1705 cm^{-1}) were selected to identify secondary protein structures. The mechanical strength was measured using a TA-ARES-controlled strain rheometer equipped with a normal force transducer. Measurements were done on wet scaffolds at room temperature (25 °C). Cylindrical scaffolds (diameter ∼6 mm; height ∼5 mm) were used for the mechanical study. UV-vis spectral analyses were performed using an Agilent diode array Cary 8454 spectrophotometer. Epifluorescence images for the in vitro cell culture experiments were captured by an Axio Observer Z1 Carl Zeiss microscope. All experiments were performed several times to confirm their reproducibility. TGA was performed using a Mettler-Toledo TG50 and SDT Q600 TG-DTA analyser under a nitrogen (N_2) atmosphere. The analysis was carried out within the temperature range of 30 °C to 750 °C, employing a ramp rate of 10 °C min^{-1}.

.

Release Kinetics Model Fitting of Vancomycin from the Sericin Scaffold

The release profile of Vancomycin (Vm) from the sericin scaffold (SE1) was analyzed using three kinetic models: zero-order release kinetics ($y = K_0 \cdot x + b_0$), first-order release kinetics ($y = K_1 \cdot e^{ax} + b_1$), and the Korsmeyer–Peppas model ($y = K \cdot x^n$), which are generally employed to describe release of drugs from solid matrices.[1–3] Here, y represents the percentage of drug release, and x denotes the release time (min). The constants include K_0 (zero-order rate constant), b_0 (intercept of the zero-order release kinetics), K_1 (first-order rate constant), b_1 (intercept of the first-order release kinetics), K (release rate constant for the Korsmeyer–Peppas model), and n (release exponent for the Korsmeyer–Peppas model). The fitting was performed using Origin software, and the corresponding linear fit curves, along with their equations, are presented in Figure S7 and Table S1.

The results indicated that the Korsmeyer–Peppas model closely aligned with the observed drug release pattern of Vm from the scaffold. The first-order model suggests that the drug is primarily adsorbed onto the inner surface of the scaffold.[4] Compared to the first-order kinetics

models, the Korsmeyer–Peppas model provided the best fit for the Vm release and showed higher Adj. R-Square. The Korsmeyer–Peppas equation applies to the initial 60% of the fractional release and helps characterize different transport mechanisms, including Fickian and non-Fickian diffusion.[5] The parameter n determines the release mechanism, where n<0.45 corresponds to Fickian diffusion, and 0.45<n<0.89 indicates non-Fickian transport. For Vm release from the scaffold, n was approximately 0.42, signifying that Fickian diffusion is the dominant mechanism. This type of normal diffusion describes the passive movement of molecules from areas of higher concentration to areas of lower concentration.

Determination of Crosslinking Density

The amount of free primary amine groups (–NH_2) in crosslinked and non-crosslinked sericin matrices was determined using a 2,4,6-trinitrobenzenesulfonic acid (TNBS) assay (from TCI Chemicals) following previous reports.[6,7] Briefly, a definite dry scaffold was treated with 0.5 mL of 4% w/v sodium bicarbonate solution. Then, 0.5 mL of freshly prepared 0.05% TNBS solution was added, and the mixture was incubated at 40 °C for 2 h. After the reaction, 1.5 mL of 6 N HCl was added to stop the reaction, and the samples were hydrolyzed at 70 °C for 4 h. The samples were cooled to room temperature, diluted with distilled water, and the absorbance was measured at 339 nm using a UV–visible spectrophotometer. A calibration curve prepared with known concentrations of glycine in 4% w/v sodium bicarbonate was used to determine the concentration of free amine groups. As a control, 4% w/v sodium bicarbonate solution without any amine was used as the sample. All measurements were carried out in triplicate.

The non-crosslinked sericin was considered to contain 100% of the available primary amine groups and was used as the free-amine concentration before reaction. The amount of reacted amine groups after crosslinking was calculated relative to this value. For crosslinking systems involving two amine groups per crosslink (assuming one BDE molecule forms a bridge between two amine groups), the crosslinking density was calculated as follows:

$$\text{Crosslinking density per unit volume}(\text{mol/cm}^3) = \frac{C_0 - C_x}{2} \times p$$

$$\text{Degree of crosslinking }(\%) = \frac{C_0 - C_x}{C_0} \times 100$$

Where, C_0 is the free amine concentration in non-crosslinked sericin (mol/g), C_x is the free amine concentration in crosslinked scaffold (mol/g), p is the density of the scaffold (g/cm³).

The obtained free amine contained in non-crosslinked sericin was about 0.39 mmol/g, and the density of the scaffolds was about 0.06 g/cm³. The calculated crosslinking densities for the crosslinked scaffolds SE1, SE2, and SE3 are presented in Table S3. An increase in crosslinking density was observed from SE1 to SE3 as BDE concentration increased. The crosslinking density showed clear correlations with water uptake, mechanical properties, and enzymatic degradation behavior (Table S3). Specifically, higher crosslink density resulted in a lower water uptake, indicating reduced porosity. This was accompanied by an increase in compressive modulus and a slower degradation rate. The obtained degree of crosslinking for SE1 is 56%, for SE2 is 67%, and for SE3 is 74%. These results confirm that the percentage of crosslinking plays a key role in regulating the structural stability and functional performance of the sericin scaffolds.

Estimation of β-sheet Content

Peak deconvolution and curve fitting of the amide I region (1600–1700 cm^{-1}) were performed to quantify the relative contributions of different secondary structures, including β-sheets, random coils, α-helices, and turns (Figure S4b). In the case of uncrosslinked sericin, the amide I band was dominated by a broad peak at around 1640 cm^{-1} primarily corresponding to random coil structures (Figure S4bi). In contrast, the crosslinked scaffolds showed clear deconvolution into multiple components. Peaks at ~1622–1625 cm^{-1} were assigned to the main β-sheet band, while peaks at ~1693–1697 cm^{-1} corresponded to antiparallel β-sheet structures, which are characteristic of methanol-induced β-sheet formation.[8,9] An additional component around ~1670 cm^{-1} was attributed to β-turn structures. The area of each fitted peak within the amide I region was integrated, and the β-sheet content was calculated by the following equation

$$\beta - \text{sheet content (\%)} = \frac{\text{Area of } \beta - \text{sheet peaks}}{\text{Total amine I area}} \times 100$$

For scaffold SE1 (Figure S4bii), the deconvoluted peaks in the amide I region were observed at ~1622 and ~1626 cm^{-1} with peak areas of 0.75 and 4.3, respectively, corresponding to the main β-sheet bands. A peak at ~1670 cm^{-1} with an area of 0.85 was assigned to β-turn structures, while a smaller peak at ~1697 cm^{-1} with an area of 0.20 corresponded to the antiparallel β-sheet component. Similarly, for scaffold SE2 (Figure S4biii), the peak at ~1622 cm^{-1} had an area of 6.15, while the peaks at ~1669 cm^{-1} and ~1693 cm^{-1} had areas of 0.50 and 0.45, respectively. In the case of scaffold SE3 (Figure S4biv), the corresponding peak areas were 7.78 at ~1622 cm^{-1}, 0.50 at ~1668 cm^{-1}, and 0.56 at ~1693 cm^{-1}. Based on this analysis, the β-sheet content was approximately 86% for SE1, 93% for SE2, and 95% for SE3."

Thermal Stability Analysis

To evaluate the thermal stability of the extracted sericin and the fabricated scaffolds, thermogravimetric analysis (TGA) was performed from 30 °C to 750 °C at a heating rate of 10 °C min^{-1}. The TGA curves exhibit two main stages of weight loss (Figure S6). The first stage, occurring between 30 °C and 200 °C, is attributed to the evaporation of physically adsorbed water associated with the protein matrix. The second stage, between approximately 200 °C and 680 °C, corresponds to the thermal degradation of the protein backbone. For the extracted sericin (Figure S6a), degradation occurred gradually, with ~10% mass loss at ~211 °C, ~60% at ~374 °C, and ~80% at ~502 °C, consistent with previous reports.[10,11] In the case of scaffold SE1 (Figure S6b), ~10% mass loss occurred at ~210 °C; however, further mass loss was observed at higher temperatures than those of extracted sericin: ~60% at 392 °C and ~80% at 575 °C. For scaffold SE2 (Figure S6c), ~10% mass loss occurred at 248 °C, ~60% at 409 °C, and ~80% at 584 °C, while for scaffold SE3 (Figure S6d) the corresponding temperatures were ~245 °C, ~470 °C, and ~625 °C. The progressive increase in the degradation temperature of the scaffolds relative to the extracted sericin indicates enhanced thermal stability resulting from the formation of a more compact, crosslinked network. Moreover, the scaffolds prepared with higher BDE concentrations exhibited greater thermal stability, further confirming the role of crosslinking in improving the structural robustness of the sericin matrix.

Tables

Table S1. The release kinetics model fitting of Vancomycin from the scaffold SE1.

Kinetics Model	Theoretical Equation	Obtained Equation	Adj. R-Square
Zero-order release kinetics	$y = K_0 \cdot x + b_0$	$y = 0.02 \cdot x + 7.8$	0.75
First-order release kinetics	$y = K_1 \cdot e^{ax} + b_1$	$y = 78.09 - 78 \cdot e\text{-}0.00155 \cdot x$	0
Korsmeyer–Peppas model	$y = K \cdot x^n$	$y = 2.23 \cdot x^{0.42}$	0.95

Table S2. The pore size variation of the scaffold with cross-linker concentration.

Scaffold No	Sericin (3 w/v%)	BDE Linker (mM)	Pore Size (µm)
SE1	1.5 mL	0.2	108 ± 25
SE2	1.5 mL	0.36	91 ± 22
SE3	1.5 mL	0.54	64 ± 18
SE4	1.5 mL	0.71	45 ± 17
SE5	1.5 mL	0.93	36 ± 15

Table S3: The crosslinking density of the sericin scaffolds along with water uptake, modulus, and enzymatic degradation rate.

Materials	Free -NH_2 in sericin (mol/g) ×10^{-5}	Unreacted free -NH_2 in scaffold (mol/g) ×10^{-5}	Reacted -NH_2 in scaffold (mol/g) ×10^{-5}	Crosslinking density (mol/cm^3) × 10^{-5}	Water uptake (w/w%)	Modulus (kPa)	*Degradation rate in Protease XIV* (w/w%)
Scaffold SE1	39 ± 1.1	17 ± 0.7	22 ± 1.3	0.73 ± 0.04	988 ± 34	11.17 ± 0.87	78 ± 2
Scaffold SE2	39 ± 1.1	13 ± 0.2	26 ± 1.2	0.86 ± 0.04	809 ± 19	11.43 ± 0.45	71 ± 3
Scaffold SE3	39 ± 1.1	10 ± 0.3	29 ± 1.2	0.96 ± 0.04	718 ± 28	12.17 ± 0.71	63 ± 4

Table S4: Comparison of mechanical properties of the sericin scaffold with reported soft skin tissues and commercial wound dressing materials.[12–17]

Materials	Modulus	Method	References
1. Epidermis 2. Dermis	1. Elastic modulus ~ 0.75-2.42 Mpa 2. Young's modulus ~ 7.33–13.48 MPa	In vitro	Biomaterials **2011**, *32*, 4670-4681
Forearm skin	Young's modulus ~ 4.75-17.99 kPa	in vivo	Medical Engineering & Physics, **2012**, *34*, 172–178
1. Epidermis (including the stratum corneum) 2. Dermis 3. Hypodermis	1. Young's modulus ~ 4 Mpa 2. Young's moduli ~ 40 kPa 3. Young's moduli ~ 15 kPa	in vivo	Acta Biomaterialia **2022**, *146*, 295–305
Commercial gauze or cotton wool	Young's modulus ~ 1 MPa - 1 GPa	In vitro	Materials Today Bio **2025**, 35, 102337
Commercial Alginate Dressings, Kaltostat®	Compressive modulus ~ 15–20 kPa	In vitro	Polymers **2023**, *15*, 3012
1. Commercial foam dressing 2. Commercial hydrogels dressing	1. Elastic modulus ~ 4-100 kPa 2. Elastic modulus ~ 15-90 kPa	In vitro	Int Wound J. **2022**, *19*, 1797–1809
Sericin scaffold	Compression modulus ~ 12 kPa	In vitro	This study

Table S5: Inhibition zones diameters at different vancomycin loading.

Weight of the loaded vancomycin/weight of the scaffold (mg/g)	Inhibition zone diameters (mm)		
	E. coli	***Bacillus subtilis***	***Methicillin-resistant Staphylococcus aureus (MRSA)***
0.01	-	-	-
0.04	-	10.5 ± 0.6	10 ± 0.00
0.16	-	15.5 ± 0.6	13.25 ± 0.5
0.31	-	16 ± 0.1	15 ± 1.0
0.63	-	16.66 ± 0.6	15.66 ± 0.6
1.25	-	17.33 ± 0.6	16.33 ± 0.6
3.12	-	19.66 ± 0.6	18.33 ± 0.6
6.25	-	21.33 ± 0.6	20.33 ± 0.6
12.5	-	23.33 ± 0.6	22.33 ± 0.6

Figures

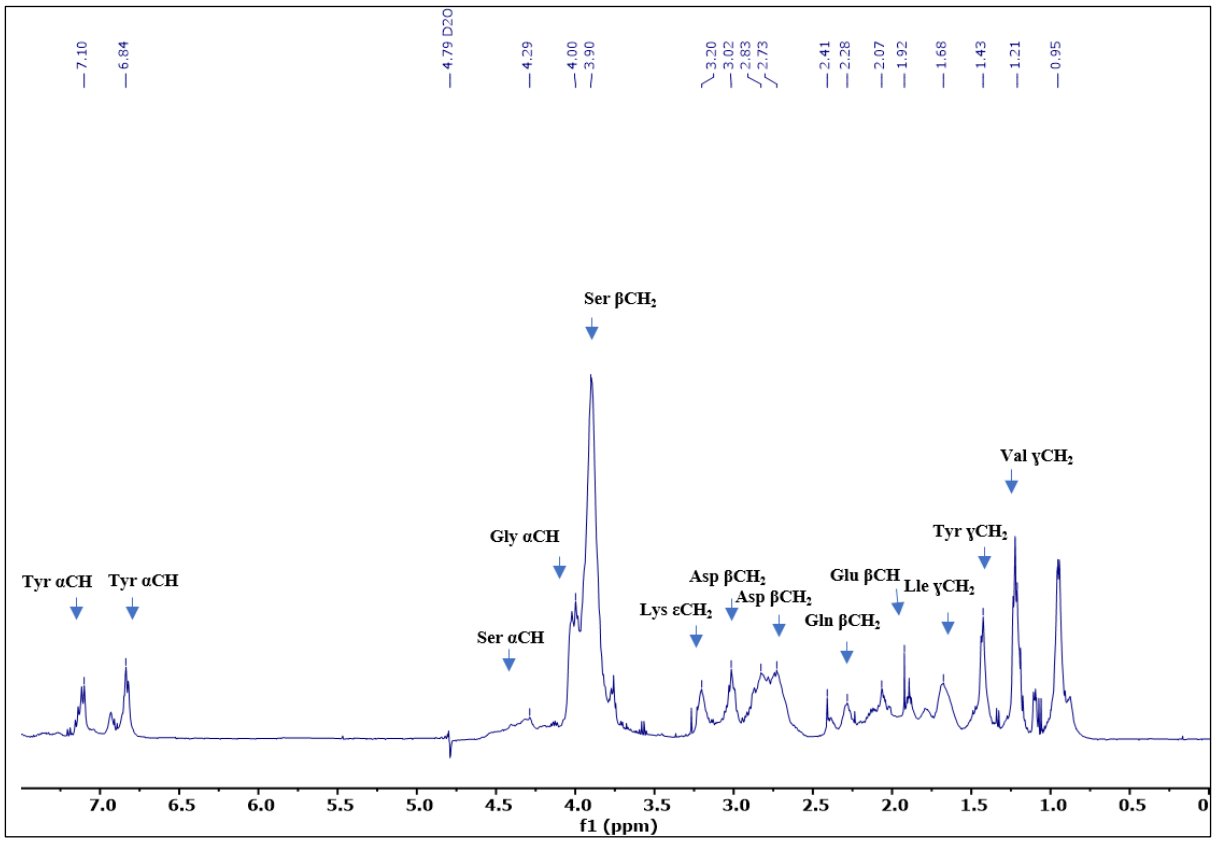

Figure S1. ^{1}H NMR of the extracted sericin in D_2O.

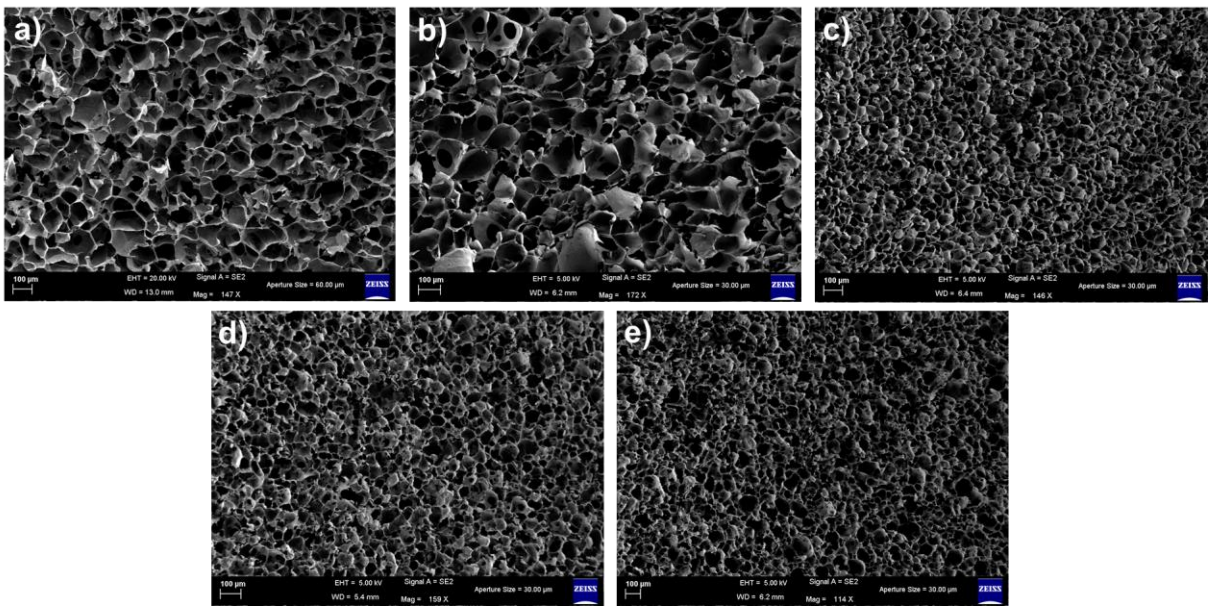

Figure S2. FESEM images of the sericin scaffold (a) SE1, (b) SE2, (c) SE3, (d) SE4, (e) SE5.

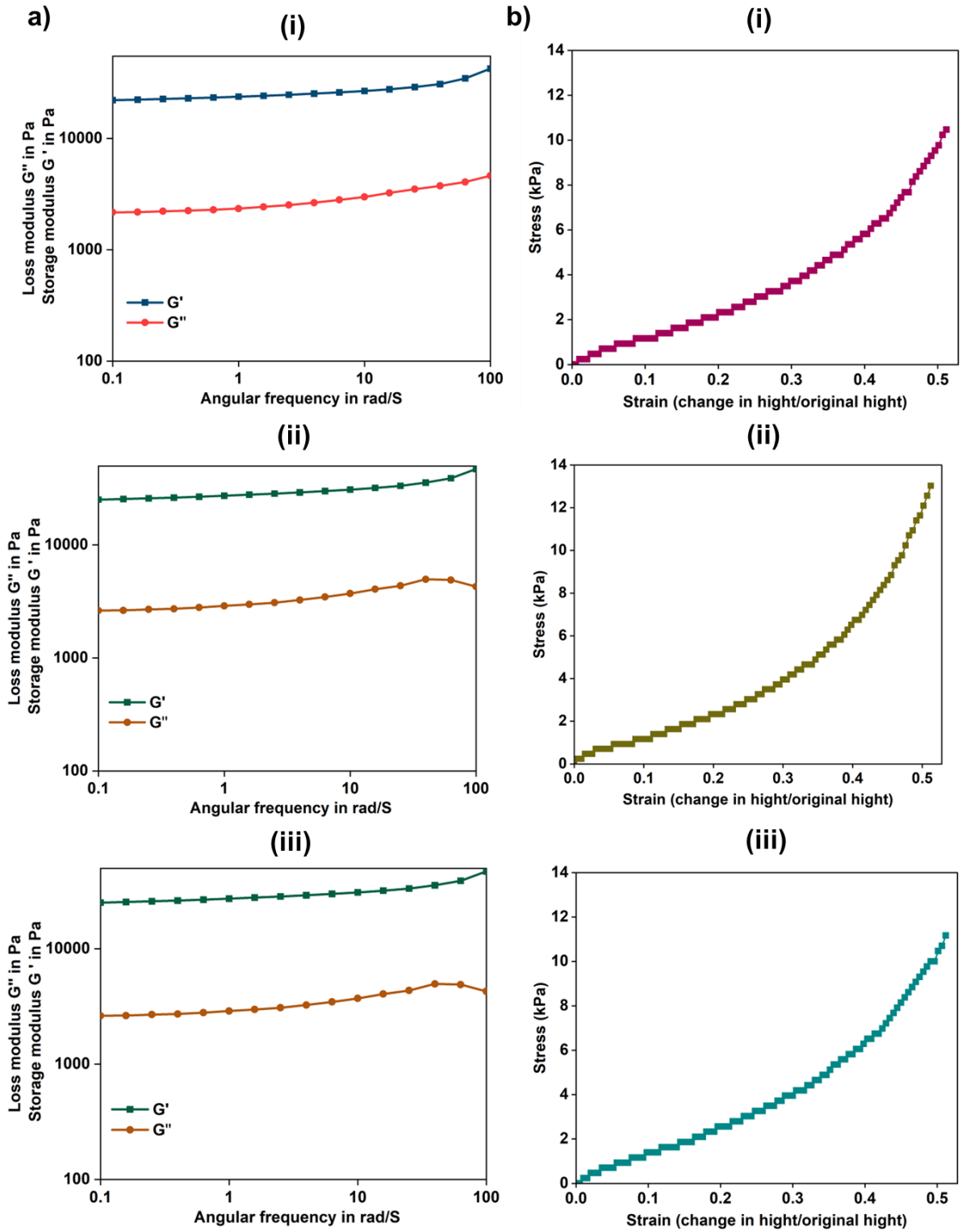

Figure S3. (a) Loss and storage modulus of the sericin scaffold (i) SE1, (ii) SE2, (iii) SE3, (b) Compressive stress-strain curve of the sericin scaffold, (i) SE1, (ii) SE2, (iii) SE3.

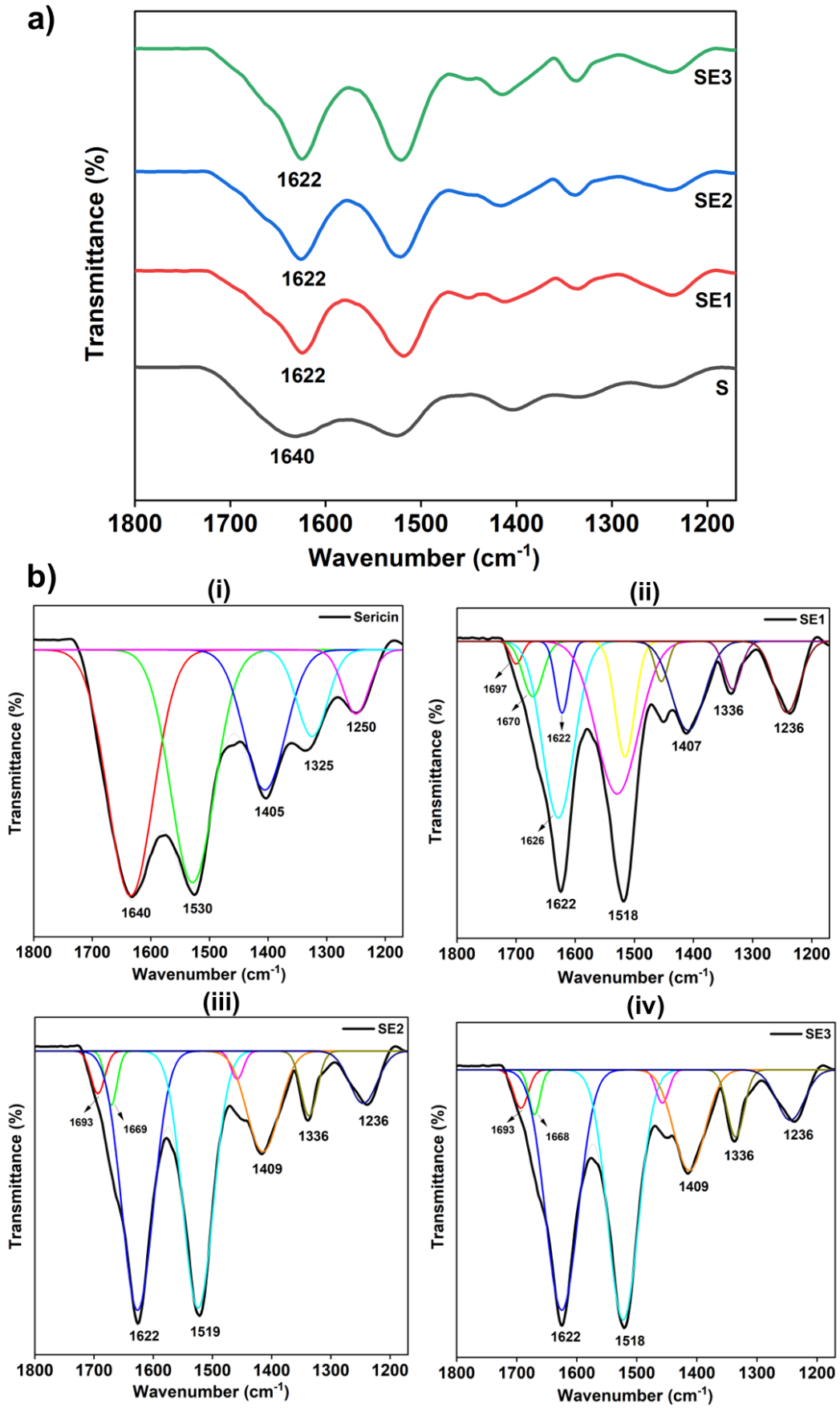

Figure S4. (a) ATR-FTIR spectrum of sericin(S) and fabricated scaffold (SE1, SE2, and SE3), (b) Deconvoluted ATR-FTIR spectrum, (i) Sericin, (ii) Scaffold SE1, (iii) Scaffold SE2, and (iv) Scaffold SE3.

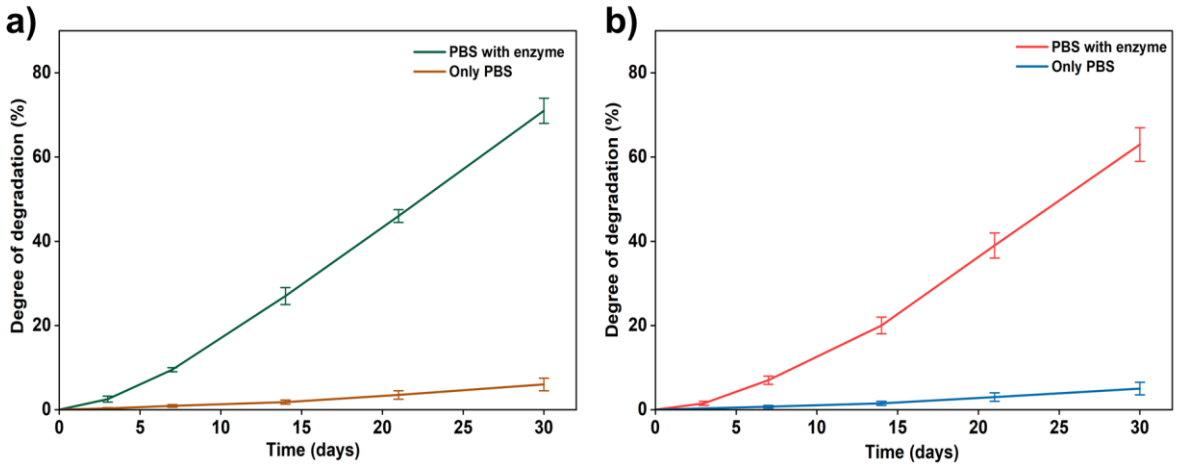

Figure S5: (a) In vitro degradation profile of the sericin scaffold SE2, (b) In vitro degradation profile of the sericin scaffold SE3.

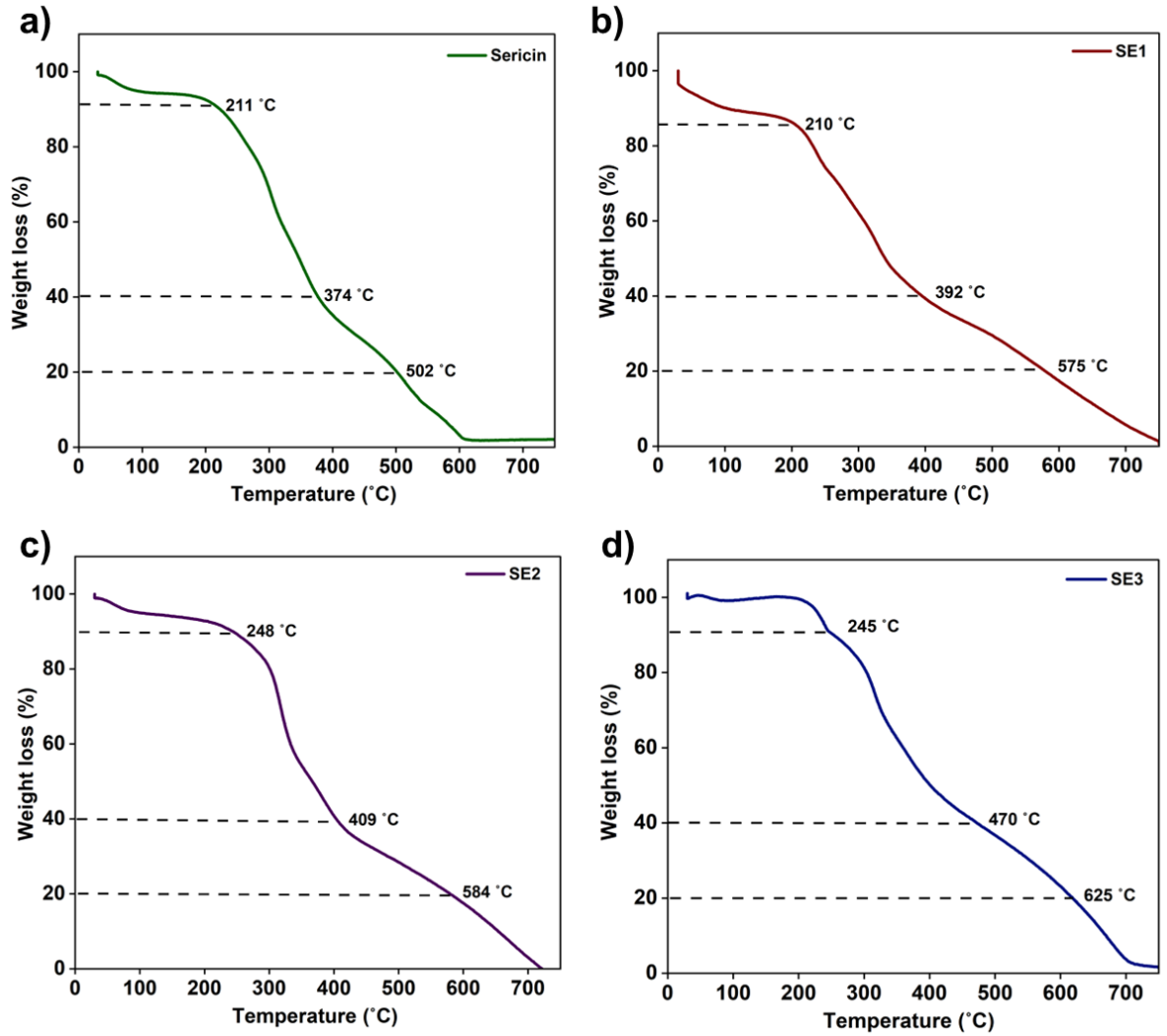

Figure S6. TGA profile, (a) Sericin, (b) Scaffold SE1, (c) Scaffold SE2, and (d) Scaffold SE3.

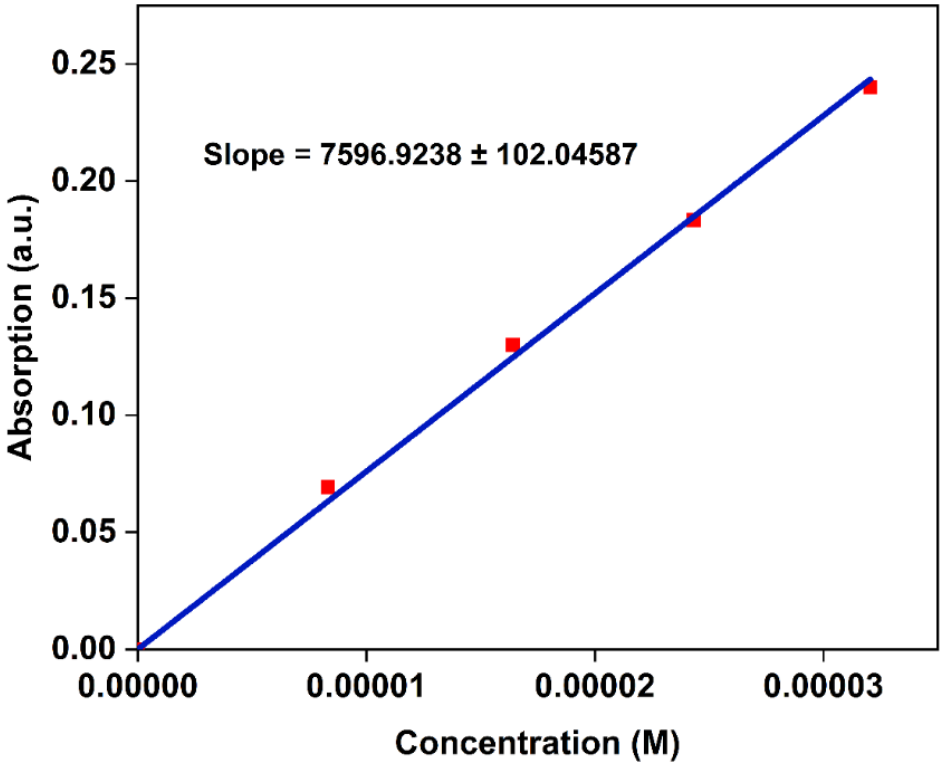

Figure S7. Calibration curve of Vancomycin in PBS (pH 7.4).

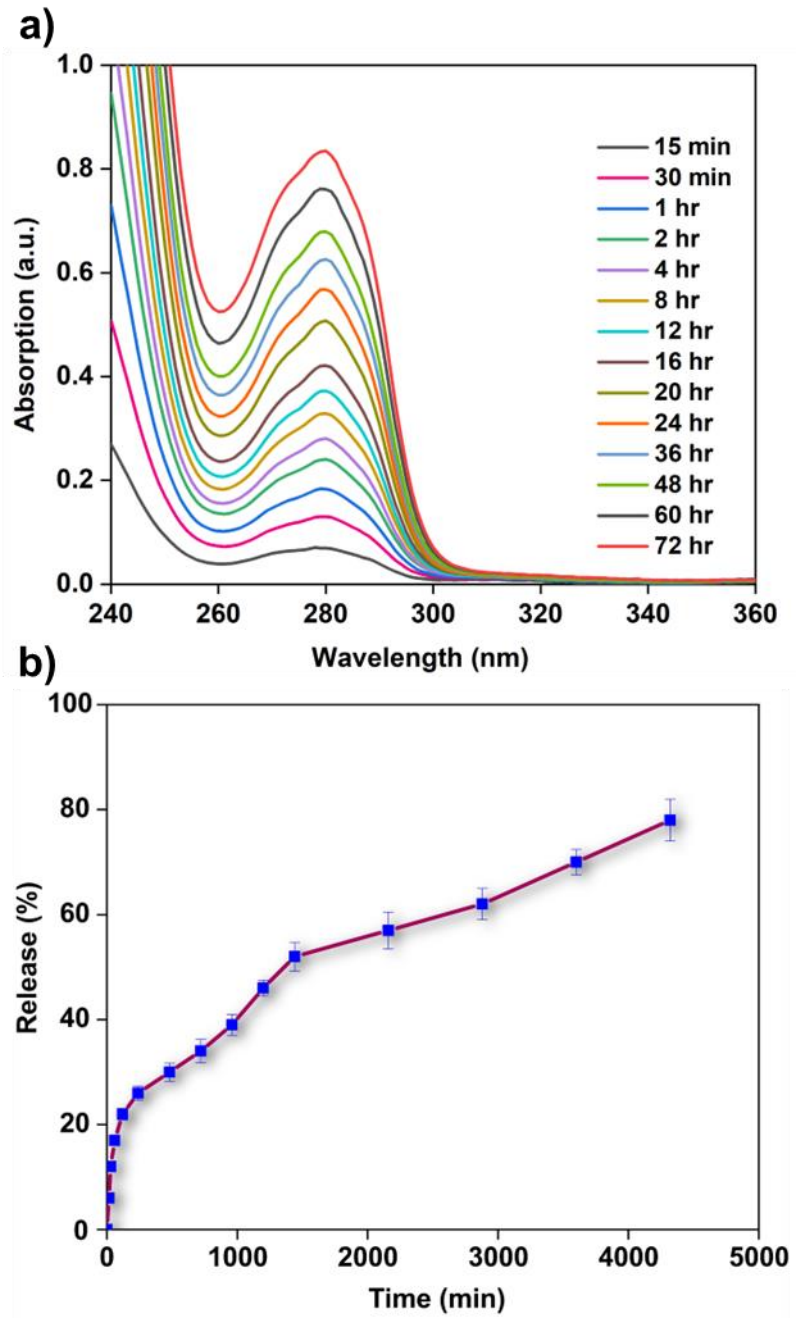

Figure S8. Release of Vancomycin over time from the sericin scaffold SE1, (a) UV-vis spectra, (b) Time vs. release profile.

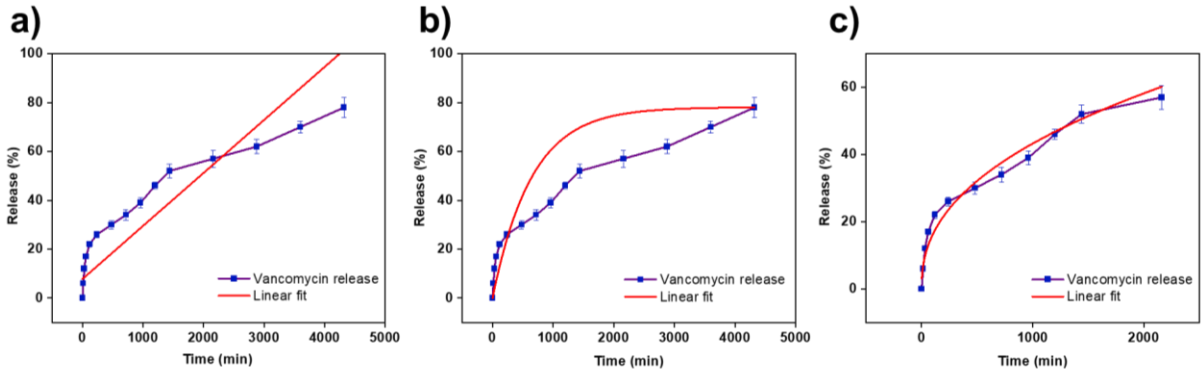

Figure S9. The release profile of Vancomycin from the sericin scaffold SE1, (a) zero-order release kinetics, (b) first-order release kinetics, (c) Korsmeyer–Peppas model.

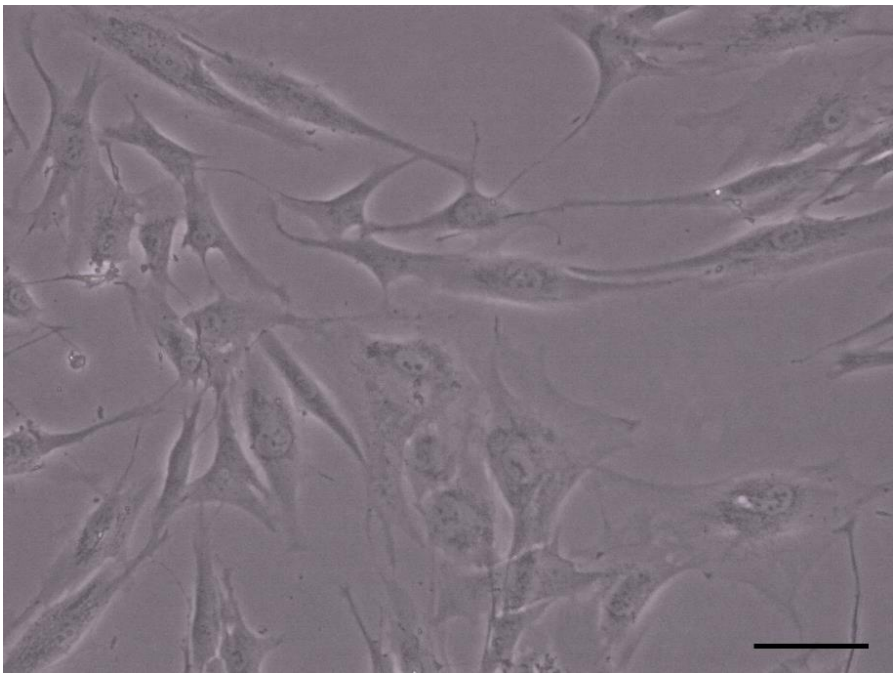

Figure S10. Microscope images of human foreskin fibroblasts (HFF-1) cells used in the experiments. Scale bars =100 µm.

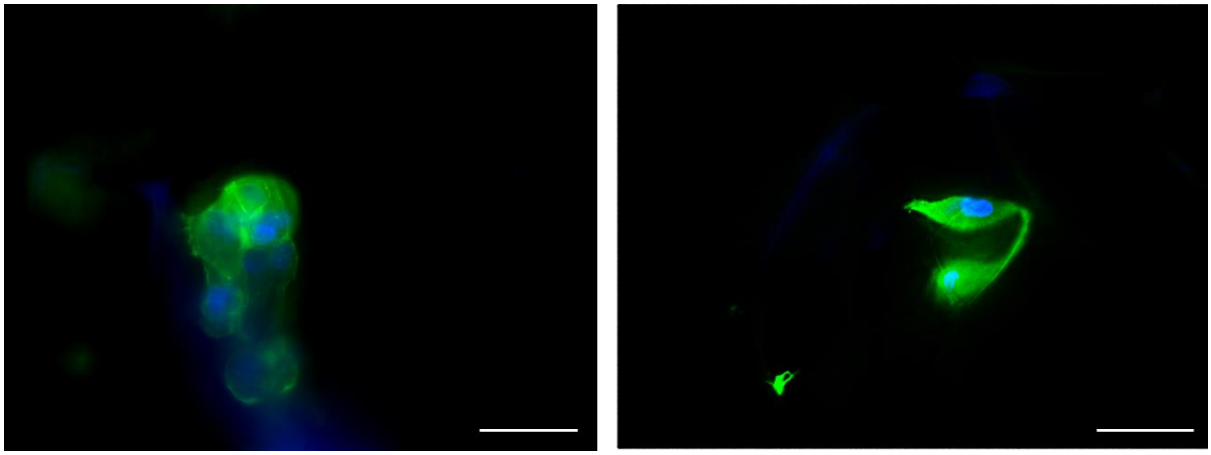

Figure S11. Epifluorescence images of the HFF cells in the scaffold SE1, stained with Alexa Fluor 488 phalloidin, and nuclei were counter-stained by DAPI at day 7th. Scale bars =100 µm.

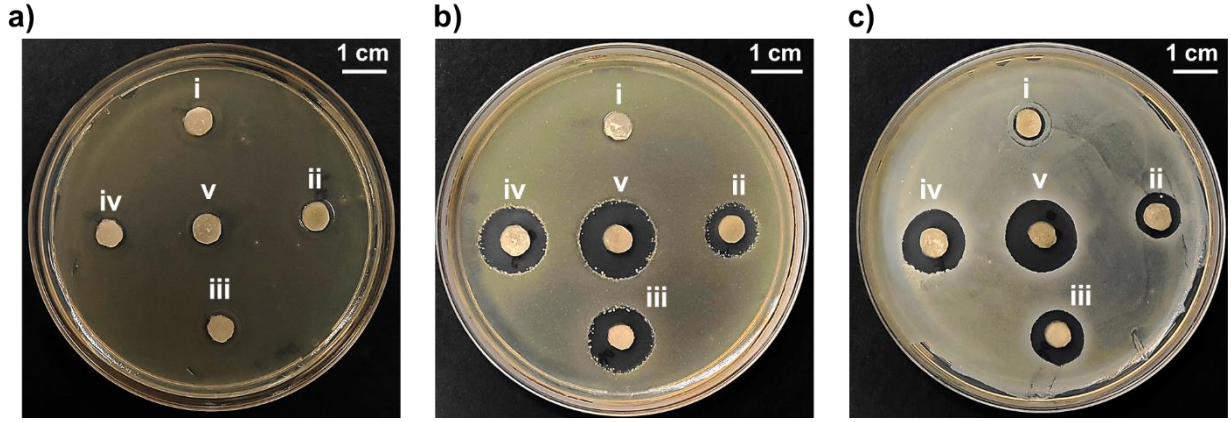

Figure S12. Bacterial zone inhibition at different vancomycin loading in the scaffold SE1, (a) *E. coli*, (b) *Bacillus subtilis*, (c) *Methicillin-resistant Staphylococcus aureus (MRSA)*, (i) 0.01 mg/g, (ii) 0.04 mg/g, (iii) 0.16 mg/g, (iv) 0.31 mg/g, (v) 0.63 mg/g.

References:

[1] W. Zhu, J. Long, M. Shi, "Release Kinetics Model Fitting of Drugs with Different Structures from Viscose Fabric" *Materials* **2023**, *16*, 3282.

[2] L. L. Lao, N. A. Peppas, F. Y. C. Boey, S. S. Venkatraman, "Modeling of drug release from bulk-degrading polymers" *International Journal of Pharmaceutics* **2011**, *418*, 28–41.

[3] R. W. Korsmeyer, R. Gurny, E. Doelker, P. Buri, N. A. Peppas, "Mechanisms of solute release from porous hydrophilic polymers" *International Journal of Pharmaceutics* **1983**, *15*, 25–35.

[4] W. Zhang, X. Wang, J. Wang, L. Zhang, "Drugs adsorption and release behavior of collagen/bacterial cellulose porous microspheres" *International Journal of Biological Macromolecules* **2019**, *140*, 196–205.

[5] S. Dash, P. N. Murthy, L. Nath, P. Chowdhury, "Kinetic modeling on drug release from controlled drug delivery systems" *Acta Pol Pharm* **2010**, *67*, 217–223.

[6] P. Aramwit, T. Siritientong, S. Kanokpanont, T. Srichana, "Formulation and characterization of silk sericin–PVA scaffold crosslinked with genipin" *International Journal of Biological Macromolecules* **2010**, *47*, 668–675.

[7] L. Salvatore, E. Calò, V. Bonfrate, D. Pedone, N. Gallo, M. L. Natali, A. Sannino, M. Madaghiele, "Exploring the effects of the crosslink density on the physicochemical properties of collagen-based scaffolds" *Polymer Testing* **2021**, *93*, 106966.

[8] X. Hu, D. Kaplan, P. Cebe, "Determining Beta-Sheet Crystallinity in Fibrous Proteins by Thermal Analysis and Infrared Spectroscopy" *Macromolecules* **2006**, *39*, 6161–6170.

[9] B. Holcombe, A. Foes, S. Banerjee, K. Yeh, S.-H. J. Wang, R. Bhargava, A. Ghosh, "Intermediate Antiparallel β Structure in Amyloid β Plaques Revealed by Infrared Spectroscopic Imaging" *ACS Chem. Neurosci.* **2023**, *14*, 3794–3803.

[10] L. K. H. Rocha, L. I. L. Favaro, A. C. Rios, E. C. Silva, W. F. Silva, T. P. Stigliani, M. Guilger, R. Lima, J. M. Oliveira, N. Aranha, M. Tubino, M. M. D. C. Vila, V. M. Balcão, "Sericin from *Bombyx mori* cocoons. Part I: Extraction and physicochemical-biological characterization for biopharmaceutical applications" *Process Biochemistry* **2017**, *61*, 163–177.

[11] S. Hossain, R. Ali, T. Hasan, "Extraction and Characterization of Sericin from Cocoon of Four Different Silkworm Races Bombyx Mori L." *European Journal of Advanced Chemistry Research* **2023**, *4*, 45–52.

[12] M. L. Crichton, B. C. Donose, X. Chen, A. P. Raphael, H. Huang, M. A. F. Kendall, "The viscoelastic, hyperelastic and scale dependent behaviour of freshly excised individual skin layers" *Biomaterials* **2011**, *32*, 4670–4681.

[13] X. Feng, G.-Y. Li, A. Ramier, A. M. Eltony, S.-H. Yun, "In vivo stiffness measurement of epidermis, dermis, and hypodermis using broadband Rayleigh-wave optical coherence elastography" *Acta Biomaterialia* **2022**, *146*, 295–305.

[14] G. Boyer, C. Pailler Mattei, J. Molimard, M. Pericoi, S. Laquieze, H. Zahouani, "Non contact method for *in vivo* assessment of skin mechanical properties for assessing effect of ageing" *Medical Engineering & Physics* **2012**, *34*, 172–178.

[15] M. Xie, Y. Xue, W. Lin, Z. Jiang, Y. Chen, Y. Pei, X. Wu, X. Xu, "Living bacteria-loaded antibacterial hydrogel-coated gauze: A revolutionary solution for multi-drug-resistant bacterial infections" *Mater Today Bio* **2025**, *35*, 102337.

[16] H. Malektaj, A. D. Drozdov, J. deClaville Christiansen, "Mechanical Properties of Alginate Hydrogels Cross-Linked with Multivalent Cations" *Polymers (Basel)* **2023**, *15*, 3012.

[17] A. Gefen, "Alternatives and preferences for materials in use for pressure ulcer prevention: An experiment-reinforced literature review" *Int Wound J* **2022**, *19*, 1797–1809.